Journal of Power Sources 248 (2014) 886–893

Contents lists available at ScienceDirect

Journal of Power Sources

journal homepage: www.elsevier.com/locate/jpowsour

Self-organized amorphous titania nanotubes with deposited graphene film like a new heterostructured electrode for lithium ion batteries

Rosa Menéndez [a], Patricia Alvarez [a], Cristina Botas [a], Francisco Nacimiento [b], Ricardo Alcántara [b,*], José L. Tirado [b], Gregorio F. Ortiz [b]

[a] Instituto Nacional del Carbón (INCAR-CSIC), Apdo. 73, 33080 Oviedo, Spain
[b] Lab. Química Inorgánica, Universidad de Córdoba, Edificio Marie Curie, Campus de Rabanales, 14071 Córdoba, Spain

HIGHLIGHTS

- A novel nanotube-TiO_2/graphene heterostructure has been synthesized.
- Graphene-self organized titania nanotube electrodes display superior lithium storage capacity than bare titania nanotubes.
- Charge–discharge possible up to 300 C rate.

GRAPHICAL ABSTRACT

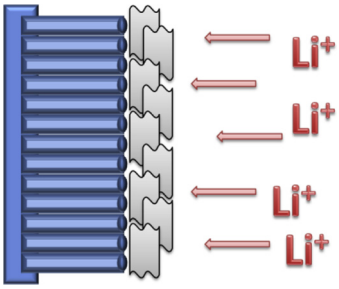

ARTICLE INFO

Article history:
Received 22 July 2013
Received in revised form
4 September 2013
Accepted 7 October 2013
Available online 15 October 2013

Keywords:
Lithium
Battery
Graphene
Titania
Ac impedance

ABSTRACT

Heterostructures composed of reduced graphene oxide and self-organized titania nanotubes (nt-TiO_2) are examined as novel electrode material for lithium-ion batteries. The novelty here resides in the deposition of a graphene-like film on self-organized nanotubes and that, as compared with previous materials, the differences in behavior are significant as the heterostructure combines previously reported advantages of self-organized nt-TiO_2 with those emerging from the graphene composites. The preparation of this nt-TiO_2/graphene hybrid electrode material is described here. The deposition of a graphene film on self-arranged amorphous nt-TiO_2 was confirmed by using SEM, Raman spectroscopy and mapping of composition. Lithium test cells display capacities that can exceed 300 mAh g^{-1} over 100 cycles and that are therefore superior to those of bare nt-TiO_2 and anatase or rutile TiO_2–graphene hybrid nanostructures. The excellent rate performance of these electrodes makes charge–discharge possible up to at least 300 C-rate. The impedance spectra show that the graphene-like film improves the interface properties in the hybrid electrode. In addition to the environmentally friendly nature of the active electrode material, the moderate working voltage offers an important safety advantage in that it protects the battery from the electroplating phenomena.

1. Introduction

Energy storage is currently a key parameter in the global economy due to the need for an efficient use of renewable energy in a variety of fields such as sustainable transportation and mobile electronics to name just two. Lithium-ion batteries are prominent electrochemical electricity storage devices that are under constant development. The future of lithium-ion batteries will probably be governed by environmental and sustainability issues and the continuous improvements in the energy and power density.

* Corresponding author. Tel.: +34 957218637; fax: +34 957218621.
E-mail address: iq2alror@uco.es (R. Alcántara).

0378-7753/$ – see front matter © 2013 Elsevier B.V. All rights reserved.
http://dx.doi.org/10.1016/j.jpowsour.2013.10.019

Table 1
Characteristics of GO determined by Raman spectroscopy, XRD and fitted results of the C1s core level XPS spectra, C/O ratio and the carbon content of the GO.

	Raman			XRD	
	W_D	W_G	I_D/I_G	d_{001}	Lc
GO	1344 cm^{-1}	1603 cm^{-1}	0.91	0.853 nm	7.48 nm
XPS					
C/O	C	Csp^2 (284.5 eV)	Csp^3 (285.5 eV)	C–O (286.1 eV)	C–O–C C=O (287.0 eV)	C(O)OH (288.5 eV)
2.3	68.6%	35.7%	9.2%	26.1%	17.3%	11.7%

In recent years, graphene and graphene derivatives have been thoroughly tested in a wide variety of applications and sometimes with surprising success. Graphene has also made headway in the field of lithium batteries about which several interesting reports can be found in the literature [1–7]. Unable to intercalate, monolayer graphene is able to store lithium ions on the surface by a non-faradic mechanism which provides similar energy densities to Li-ion batteries but with even higher power densities [2]. In conjunction with other electroactive materials, hybrid nanostructures provide extremely high capacities. Insertion, alloying and conversion active oxide materials have been tested. Chen et al. recently reported graphene wrapped SnCo nanoparticles [8]. Conversion electrodes such as cobalt [9], manganese [10], iron [11], and nickel [12] oxides display a highly improved electrochemical behavior when wrapped with graphene layers, which yields capacities close to those of Li–Sn intermetallics [13]. An insertion electrode material such as anatase TiO_2 doubles its capacity at high rates when a graphene network is embedded in the oxide electrode [14]. The encapsulation of TiO_2 nanoparticles with carbon has been proposed [15]. A composite of single-wall carbon nanohorns and nanoporous anatase TiO_2 was proposed by Xu et al. [16].

Titanium dioxide in the form of nanoparticles can exhibit superior electrochemical performance because of the short diffusion path and more sites for lithium accommodation [17]. Self-organized TiO_2 nanotubes (nt-TiO_2) are known to be prepared by anodization procedures [18], and were recently found to perform very well in lithium microbatteries, particularly before being crystallized into an anatase structure [19–21]. Further studies have shown how to combine this material in nanocomposites with other alloying (Sn) [22] and conversion (Fe_2O_3) [23] electrode materials.

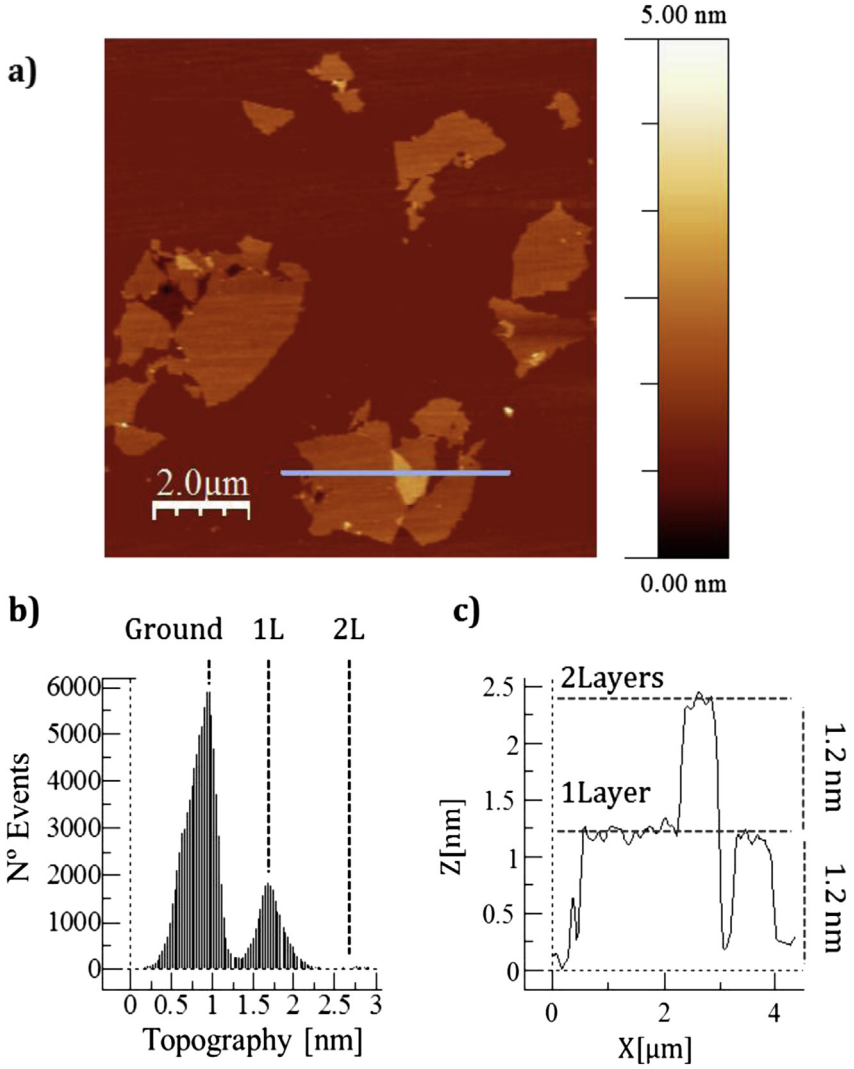

Fig. 1. (a) AFM image of GO, where the horizontal line indicates the sections corresponding to the trace shown on the right. (b) Histogram showing the height distributions of the sheets analyzed. (c) Graphene layer number as a function of the distance.

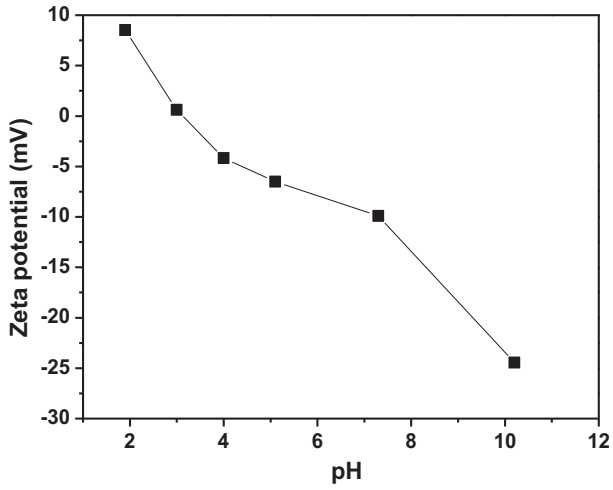

Fig. 2. Measured zeta-potential value as a function of pH for reduced graphene oxide.

As a result, the areal capacity could be enhanced up to ten times that of pure nanotubes. However, these nanocomposites have been penalized by a high irreversibility in the first cycle and a moderate rate performance. Mancini et al. proposed to coat mesoporous anatase with Cu or Sn to improve the kinetics of Li insertion/extraction [24].

The aim of the present work is to evaluate nt-TiO_2/graphene heterostructures that can combine the environmentally benign nature of both components with an enhanced electrochemical response in advanced lithium batteries. The preparation route makes use of the electrophoretic deposition properties of graphene that were recently found to be useful in preparing graphene/platinum electrocatalytic electrodes [25] and graphene/TiO_2 photoelectrodes [26]. We have found that the deposition of a graphene film on the surface of nt-TiO_2 results in a net improvement of the electrochemical properties and the mechanism is discussed by using ac impedance spectroscopy.

2. Experimental

2.1. Preparation of graphene oxide and reduced graphene oxide

Graphene oxide (GO) was prepared from a synthetic graphite by a modification of the Hummers method [27]. The main characteristics of the graphene oxide sample are shown in Table 1 and Fig. 1. To obtain graphene, the reduction of graphene oxide with hydrazine was carried out [25]. For this purpose, 0.04 mL of 80% hydrazine aqueous solution and 0.28 mL of 30% aqueous ammonia was added to 40 mL of aqueous GO solution in a closed vessel which was then placed in a water bath at 100 °C for 2 h. The brown GO solution tuned black upon reduction.

2.2. Preparation of titania nanotubes

To prepare self-organized TiO_2 nanotubes, anodization of titanium foils from Aldrich with a thickness of 0.127 mm and 99.7% purity was employed. Firstly, the Ti foil was cut and cleaned with ethanol–water mixtures in an ultrasound bath. Then, electrochemical anodization was carried out at room temperature by using a constant voltage of 60 V for 120 min and was performed using a piece of Ti (0.888 cm^2) as the working electrode, platinum foil as the counter electrode, and an electrolyte consisting of 3 wt.% NH_4F and 2 wt.% water in ethylene glycol, as described in elsewhere [20]. The voltage was controlled by an Agilent B2911A apparatus. The weight of nt-TiO_2 per surface area was estimated by separating the nanotube film from the Ti substrate with intense and prolonged ultrasonication [21,26].

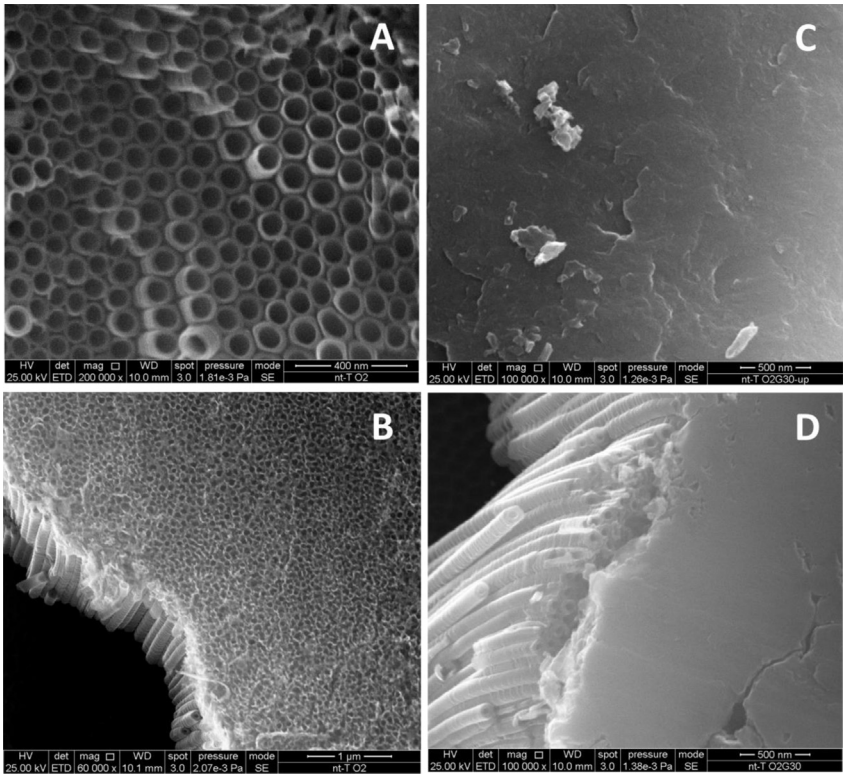

Fig. 3. Selected SEM images of (A, B) bare nt-TiO_2 and (C, D) nt-TiO_2/graphene heterostructure.

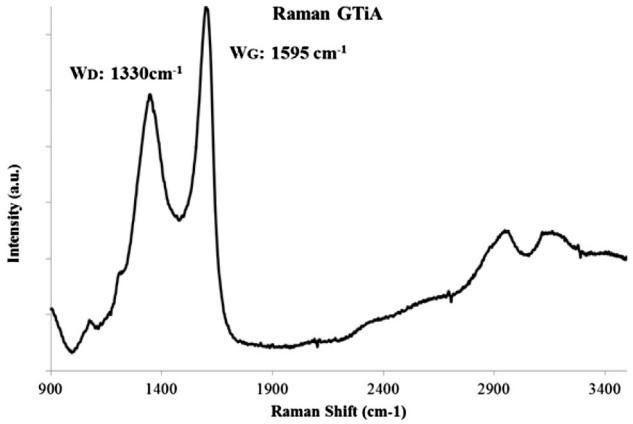

Fig. 4. Raman spectrum of the nt-TiO_2/graphene heterostructure.

2.3. Preparation of titania nanotube/graphene heterostructure

The electrophoretic deposition of graphene on the surface of self-organized nanotubes was carried out at room temperature using a two-electrode cell configuration and an Agilent B2911A apparatus with a 4 V Pt counter electrode for 30 min. For the sake of comparison, an excess of graphene was deposited for 90 min, and this is refereed here like in-excess deposited graphene. The graphene obtained by reduction of GO with hydrazine exhibits a negative value of zeta-potential at pH greater than 4 (Fig. 2). A pH value of 12 was used for the electrophoresis experiments carried out in this work, which represents a similar behavior than that observed for colloidal graphene oxide. This implies that the reduced graphene oxide will move under an electric field toward the positively charged electrode to form a layer, therefore producing the nt-TiO_2/graphene heterostructure [25,28,29].

2.4. Characterization

XRD patterns were recorded in a Siemens XRD instrument with CuKα radiation. Field emission Scanning Electron Microscope (SEM) images were obtained using a QUANTAN FEG 650 FEI operating at 25 kV. Mappings of composition were obtained in a in a Scanning Electron Microscope (SEM) JSM-6300 instrument equipped with an energy dispersive X-ray instrument equipped with microanalysis probe (EDAX detector). Raman spectra were recorded from 750 to 3500 cm^{-1} on a Renishaw 2000 Confocal Raman Microprobe (Rhenishaw Instruments, England) using a 514.5 nm argon ion laser.

2.5. Electrochemical measurements

The electrochemical performance of the prepared electrodes was studied by means of experiments in lithium Swagelok-type test cells, assembled in an argon-filled glovebox in which the moisture content and oxygen level were below 2 ppm. The electrolyte was 1 M $LiPF_6$ in ethylene carbonate (EC) and diethylcarbonate (DEC) solvents mixture (EC:DEC = 50:50) which was embedded in a Whatman glass microfiber that acted as a separator. For the galvanostatic discharge/charge experiments, a constant current density of 0.1 mA cm^{-2} (equivalent to ca. C/3, where C/*n* means *n* hours for each discharge) was applied to the assembled cells and using two different potential ranges: 1.0–2.6 V and 0.0–3.0 V. For this purpose an Arbin potentiostat/galvanostat multichannel system was employed. Alternatively, a variable current density was imposed to study the rate performance. For these experiments no additives like poly(vinyl difluoride), that act as binder agents, nor any carbon black (conductive agent) were used. To evaluate the gravimetric capacities, the films were subjected to ultrasounds in order to separate the nanotubes from the Ti substrate, and weighed again. Thus, the active material mass (nt-TiO_2 and graphene) was ca. 1.03(2) mg cm^{-2}. The impedance spectra were recorded by using three-electrode cells with T-configuration in a VMP instrument.

3. Results and discussion

3.1. Characterizations of the electrode materials

The field-emission SEM micrographs of nt-TiO_2 obtained by anodization of Ti foil show the nanotubes self-arrangement and their open mouths (Fig. 3A, B). The nanotube diameter of is about 50–80 nm, while the length is about 5 μm. After deposition of graphene the micrographs show that the mouths of nt-TiO_2 have

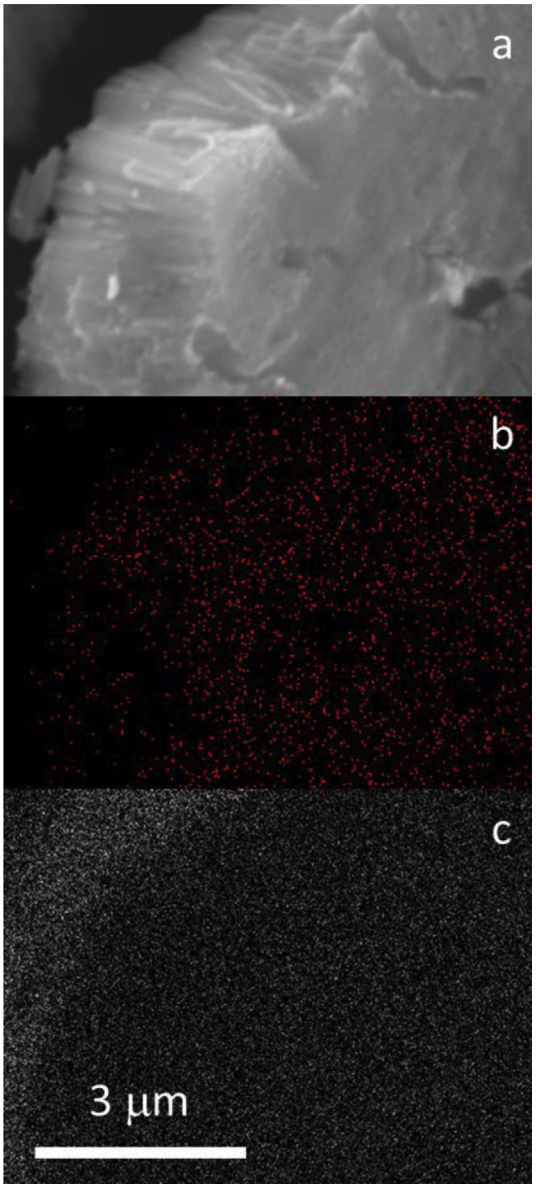

Fig. 5. SEM micrograph of the nt-TiO_2/graphene heterostructure (a) and correspondent mappings of composition (EDAX-type detector of X-ray radiation) for carbon (b) and titanium (c).

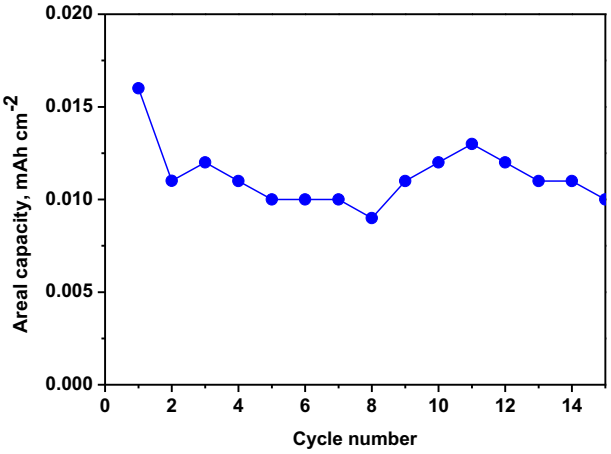

Fig. 6. Areal capacity vs. cycle number in lithium cell for an electrode of a graphene-like film electrophoretically deposited during 30 min on a flat Ti metal substrate (without previous anodization of Ti). Potential range: 0.01–3.0 V. Current density: 16 μA cm^{-2}.

been covered with a flat surface of ca. 100 nm of thickness (Fig. 3C, D). The titania nanotubes remain XRD-amorphous after graphene deposition (not shown). The presence of graphene in the heterostructure was further corroborated with the Raman spectra showing the typical D and G bands (Fig. 4), irrespectively of the fact that the broadening of the bands and the relative intensity I_G/I_D can be affected by the method used for reducing graphene oxide to obtain films or nanomaterials based on graphene [30–35]. On the other hand, the high ratio I_G/I_D is related to high electrical conductivity [35]. The mappings of composition (Fig. 5) agree well with the presence of a subtle carbon film deposited on the surface of the self-arrangement of titania nanotubes.

Henceforth, the self-arrangement of nt-TiO_2 is covered with a submicrometric graphene-like film while the incorporation of graphene within the nanotube cavity is not expected. After deposition of graphene on nt-TiO_2, the heterostructure can be refereed like nt-TiO_2/graphene electrode material. This carbon film modifies the electrochemical properties of the electrode material in lithium cell like is discussed below.

3.2. Electrochemical properties

Firstly, for the sake of comparison, the electrochemical behavior of a graphene film electrophoretically deposited on flat Ti was studied (Fig. 6). The relative stability in capacity upon cycling of the graphene layer is also observed in the cycling experiments. The resulting reversible capacity in lithium cell of this Ti/graphene electrode is ca. 0.01 mAh cm^{-2} (Fig. 6). This capacity value represents the areal capacity of the deposited graphene-like film, refereed to the apparent or external area of the electrode [20,21]. Taking into account that, after anodization of Ti, the graphene-free nt-TiO_2 film has a capacity of 0.60 mAh cm^{-2}, the contribution of the graphene film to the total capacity of the nt-TiO_2/graphene electrode is expected to be significantly lower than the differences between bare nt-TiO_2 and nt-TiO_2/graphene. Thus, the small amount of reduced graphene deposited on the surface of the electrodes seems to discount that the graphene film contributes significantly to the total gravimetric capacity of nt-TiO_2/graphene.

The charge–discharge cycles in lithium test cells were recorded by using two different potential windows for both bare nt-TiO_2 and nt-TiO_2/graphene heterostructure. The charge–discharge profiles recorded at a current density of 0.1 mA cm^{-2} and shown in Fig. 7 are all characteristic of amorphous nt-TiO_2. The lower cut-off voltage at

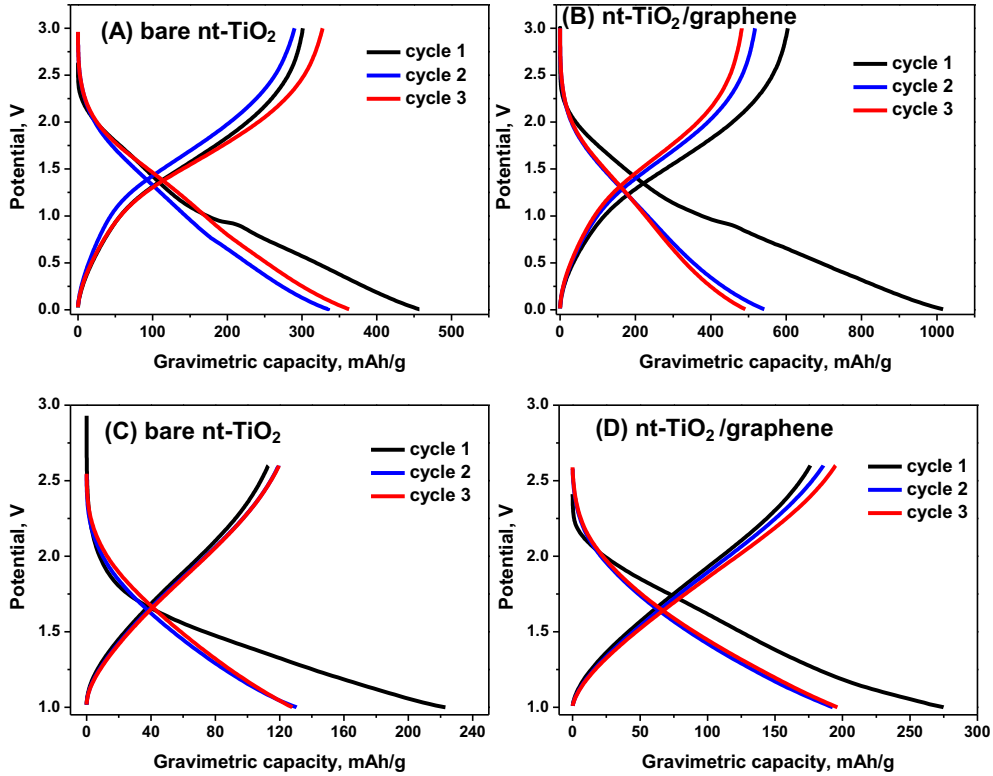

Fig. 7. Galvanostatic charge–discharge curves of lithium test cells recorded at 0.1 mA cm^{-2} of current density using like electrodes bare nt-TiO_2 (A and C) and nt-TiO_2/graphene heterostructure (B and D) in the 0.01–3.0 V (A and B) and 1.0–2.6 V (C and D) potential windows.

1.0 V is commonly used in the study of crystalline nt-TiO_2-based electrodes, as the flat intercalation voltage profile of anatase appears at ca. 1.8 V [20,21]. The amorphous character of the used nt-TiO_2 prevents the formation of extended plateaus, irrespectively of the small and irreversible pseudoplateau observed at ca. 1.0 V in the first discharge process that may be due to crystallization processes or irreversible reactions with traces of water trapped in the nanotubes [20,21,36]. Possible pseudocapacitive contributions can also be expected above 1.0 V. Thus, Dunn and co-workers found that the amount of charge stored from lithium intercalation processes decreases as the particles become smaller, and that this fact increases the capacitive contribution [37]. However, the possible contribution of surface reactions to charge storage in amorphous TiO_2 which results in the partially reversible formation of Li_2O have also been suggested as being due to the formation of Ti peroxide on the nanoparticle surface [38]. The complete conversion reaction to Ti and Li_2O should not be expected as suggested in the literature. In addition, the capacity of amorphous nt-TiO_2 can increase when the lower potential limit is decreased down to 0.0 V [20]. The higher capacity and better stability of amorphous nanostructures are clear advantages compared to anatase nt-TiO_2 [19]. In addition, the use of a wide potential window (0.1–3.0 V) also has been proposed for nanosized TiO_2 rutile [39]. The cycling stability remains nearly unaffected in subsequent cycles even in the case of a low-voltage limit (Figs. 7 and 8). In this case, the total capacity increases, leading to values well above the $Li_{0.5}TiO_2$ limit usually found for anatase and over 1.0 V. When comparing bare nt-TiO_2 electrodes (Fig. 7A and C) with the nt-TiO_2/graphene heterostructures (Fig. 7B and D), it is worth noting the significantly higher initial and reversible capacities for nt-TiO_2/graphene. The inefficiency of the first cycle when cycled down to the 0.0 V of the heterostructure is largely reduced by increasing the lower cut-off voltage.

The excellent capacity retention on the prolonged cycling of the heterostructure is also highlighted in the plots of capacity vs. number of cycles in Fig. 8A. Capacities values over 200 mAh g^{-1} are

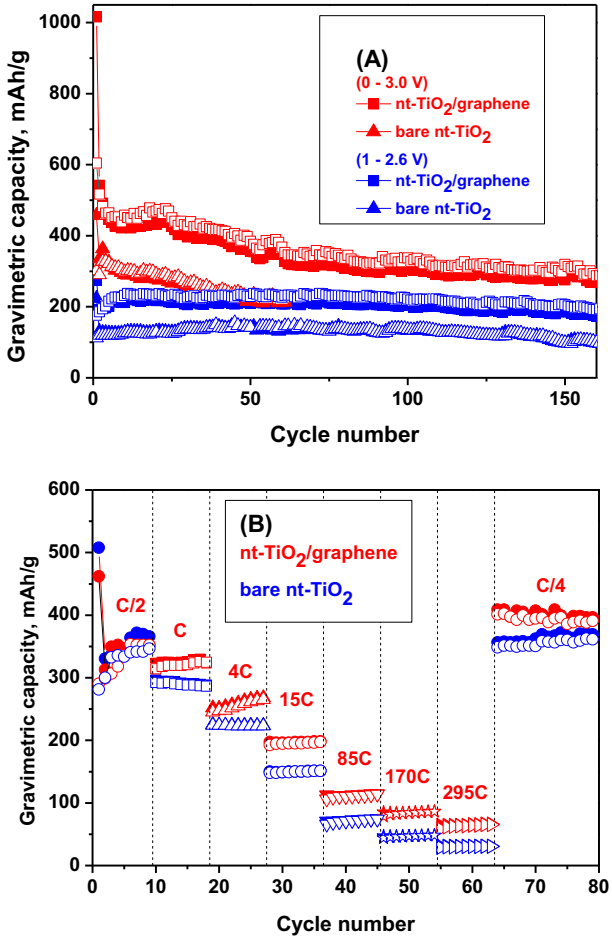

Fig. 8. Cycling performance of bare nt-TiO_2 and nt-TiO_2/graphene heterostructure: (A) at 0.1 mA cm^{-2} of current density in the 0.01–3.0 V (red color) and 1.0–2.6 V (blue color) potential ranges, and (B) at variable rate in the 1.0–2.6 V potential range. The C-rate values correspond to the heterostructured electrode. Open symbols: charge. Filled symbols: discharge. (For interpretation of the references to color in this figure legend, the reader is referred to the web version of this article.)

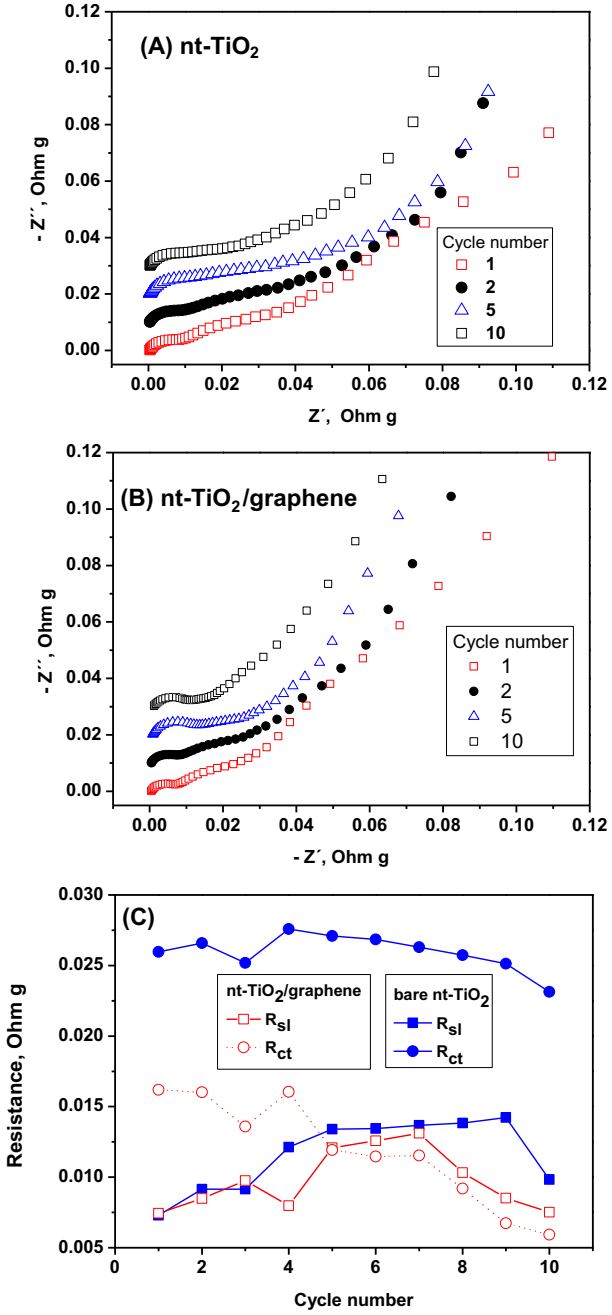

Fig. 9. Impedance spectra of (A) bare nt-TiO_2, and (B) nt-TiO_2/graphene heterostructure recorded at several cycle number. (C) Obtained values of R_{sl} and R_{ct}. The spectra were recorded at 1.0 V vs. Li reference electrode and are reported normalized for the mass loading.

retained after 100 cycles for 1.0–2.6 V of potential range and over 300 mAh g^{-1} for 0.0–3.0 V. These values are well above these of bare nt-TiO_2 and reasonably high in comparison with those reported for anatase or rutile TiO_2–graphene hybrid nanostructures [11]. In the case of wider potential windows the values are very high. At this point it is worthwhile recalling the different contributions mentioned above. In particular, a pseudocapacitive contribution through the formation of surface Li_2O is probably the origin of the extended capacity observed. However, as pointed out previously [29], this process is only partly reversible, and the capacity for retention is slightly poorer, compared to the same material in the 1.0–2.6 V potential range.

Fig. 8B compares the rate performance of bare nt-TiO_2 and that of nt-TiO_2/graphene heterostructure. In the latter case, capacities of around 200 mAh g^{-1} are found at 15 C, while values of 100 mAh g^{-1} are visible at rates as high as 85 C. Even for extremely high rates close to 300 C, significant capacities above 50 mAh g^{-1} are visible which involve that the cell could be charged in a few seconds. The recovery of the cell's capacity by decreasing the kinetics is also evident from Fig. 8B. On the other hand, in Fig. 8B, the gravimetric capacity value in the first discharge is slightly higher for bare nt-TiO_2 than nt-TiO_2/graphene and after further cycles it becomes smaller. Thus, the irreversible processes due to electrolyte consumption and water molecules trapped in the titania nanotubes can contribute to the initial activation processes.

In order to gain further insight into the surface phenomena involved in the full heterostructure, three-electrode cells, with two lithium electrodes as reference and working electrodes, respectively, were used. The recorded impedance spectra are depicted in Fig. 9. By using a wide frequency range, the different resistances (R), constant phase elements (Q) and Warburg element (W) can be estimated from the real (Z') and imaginary (Z'') part of the impedance spectra. R_e represents the total ohmic resistance of the electrodes, electrolyte, separator and electrical contacts. The R_e values were similar for both the bare nt-TiO_2 and the nt-TiO_2/graphene heterostructure. The equivalent circuit $[R_e(R_{sl}Q_{sl})(R_{ct}W)Q_{ct}]$ was found to fit very well the spectra with two semicircles of both bare nt-TiO_2 and the nt-TiO_2/graphene heterostructure. The diameter of the semicircle in the high frequency range is related to the surface layer resistance (R_{sl}) at the electrode surface including the SEI layer, and R_{ct} can be ascribed to the charge-transfer resistance. In bare nt-TiO_2, while R_{ct} values showed little changes from one cycle to another, the R_{sl} values tend to increase with the number of cycles (Fig. 9C). In contrast, for the nt-TiO_2/graphene the R_{ct} values are significantly lower and tend to decrease from the first to the tenth cycle. The values of R_{sl} are more stable for the nt-TiO_2/graphene. These results offer evidence of that the graphene film improves the interface properties of the electrode. For the sake of comparison, the R_{sl} values of a graphene film deposited on non-anodized Ti (Fig. 10) are similar to those of bare nt-TiO_2 and the nt-TiO_2/graphene heterostructure (8–11 Ω cm^{-2}). Provided that the formation of an SEI in nt-TiO_2 is also assumed [40,41], R_{sl} represents basically the resistance of the SEI. The R_{sl} results demonstrate that the graphene layer does not have a marked effect on the resistance of the SEI layer. In the case of R_{ct}, the value for the heterostructure is ascribed mainly to the charge transfer to nt-TiO_2. The significant decrease in R_{ct} from bare nt-TiO_2 to the heterostructure would involve that the graphene film improves the electrical contact of the nanotubes. This phenomenon is particularly favored by the uniform electrical contact of graphene with the self-organized nanostructure, as compared with non-organized nanotubes. This in turn is probably the origin of the excellent capacity utilization and cycling performance at high rates of nt-TiO_2/graphene heterostructure. As compared with previous materials, the differences in behavior are significant as the heterostructure combines previously reported advantages of self-organized nt-TiO_2 [10] with those emerging from the graphene composites [8,20,21].

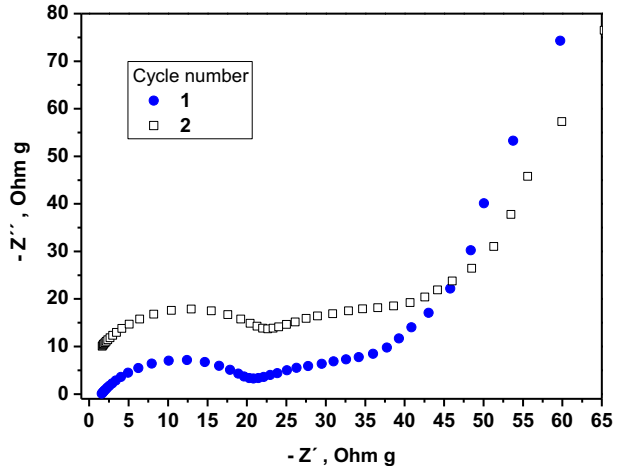

Fig. 10. Impedance spectra of a graphene layer electrophoretically deposited during 5 h on a Ti substrate without previous anodization (in-excess deposited graphene).

4. Conclusion

Heterostructures at the nano scale consisting of self-organized TiO_2 nanotubes on a Ti current collector and graphene layers coupled by electrophoresis provide a unique electrode material for advanced lithium ion batteries and microbatteries. The capacities achieved in the 1.0–2.6 V range are higher than any other TiO_2-based electrode previously reported. The absence of binding additives could provide highly effective energy densities. The extraordinary rate performance of these electrodes ensures a very fast charge–discharge capability that will be of great interest in future high power density full cells. The improved behavior results from a clear reduction in charge transfer resistance within the heterostructure. Furthermore, the moderate working voltage of the electrode offers an important advantage that will allay current safety concerns associated with electroplating and overcharging of conventional Li-ion batteries. This advantage together with the environmental and health benefits associated with the components of this battery brings the possibility of clean and efficient batteries closer to realization.

Acknowledgments

The authors are indebted to MEC (MAT2011-22753), Junta de Andalucía (FQM288) and MICINN (CONSOLIDER INGENIO 2010, Ref. CSD2009-00050) for financial support. Dr Patricia Alvarez and Dr. Gregorio Ortiz thanks MICINN for their respective Ramon y Cajal contracts. Cristina Botas acknowledges a fellowship from FICYT (Gobierno del Principado de Asturias). Authors are indebted to Dolores Casal for SEM facilities.

Appendix A. Supplementary data

Supplementary data related to this article can be found at http://dx.doi.org/10.1016/j.jpowsour.2013.10.019.

References

[1] P. Guo, H. Song, X. Chen, Electrochem. Commun. 11 (2009) 1320–1324.
[2] B.Z. Jang, C. Liu, D. Neff, Z. Yu, M.C. Wang, W. Xiong, A. Zhamu, Nano Lett. 11 (2011) 3785–3791.

[3] G. Kucinskis, G. Bajars, J. Kleperis, J. Power Sources 240 (2013) 66–79.
[4] A. Bhaskar, M. Deepa, T.N. Rao, U.V. Varadaraju, J. Power Sources 216 (2012) 169–178.
[5] L. Tao, J. Zai, K. Wang, H. Zhang, M. Xu, J. Shen, Y. Su, X. Qian, J. Power Sources 202 (2012) 230–235.
[6] X. Zhu, Y. Zhu, S. Murali, M.D. Stoller, R.S. Ruoff, J. Power Sources 196 (2011) 6473–6477.
[7] H. Zhao, L. Pan, S. Xing, J. Luo, J. Xu, J. Power Sources 222 (2013) 21–31.
[8] P. Chen, L. Guo, Y. Wang, J. Power Sources 222 (2013) 526–532.
[9] S. Yang, X. Feng, S. Ivanovici, K. Müllen, Angew. Chem. Int. Ed. 49 (2010) 8408–8411.
[10] H. Wang, L.F. Cui, Y. Yang, H.S. Casalongue, J.T. Robinson, Y. Liang, Y. Cui, H. Dai, J. Am. Chem. Soc. 132 (2010) 13978–13980.
[11] G. Zhou, D.W. Wang, F. Li, L. Zhang, N. Li, Z.S. Wu, L. Wen, G.Q. Lu, H.M. Cheng, Chem. Mater. 22 (2010) 5306–5313.
[12] Y.J. Mai, S.J. Shi, D. Zhang, Y. Lu, C.D. Gu, J.P. Tu, J. Power Sources 204 (2012) 155–161.
[13] S.M. Paek, E.J. Yoo, I. Honma, Nano Lett. 9 (2009) 72–75.
[14] D. Wang, D. Choi, J. Li, Z. Yang, Z. Nie, R. Kou, D. Hu, C. Wang, L.V. Saraf, J. Zhang, I.A. Aksay, J. Liu, ACS Nano 3 (2009) 907–914.
[15] V.G. Pol, S.H. Kang, J.M. Calderon-Moreno, C.S. Johnson, M.M. Thackeray, J. Power Sources 195 (2010) 5039–5043.
[16] W. Xu, Z. Wang, Z. Guo, Y. Liu, N. Zhou, B. Niu, Z. Shi, H. Zhang, J. Power Sources 232 (2013) 193–198.
[17] J.S. Chen, X.W. Lou, J. Power Sources 195 (2010) 2905–2908.
[18] J.M. Macak, H. Tsuchiya, P. Schmuki, Angew. Chem. Int. Ed. 44 (2005) 2100–2102.
[19] G.F. Ortiz, I. Hanzu, T. Djenizian, P. Lavela, J.L. Tirado, P. Knauth, Chem. Mater. 21 (2009) 63–67.
[20] J.R. González, R. Alcántara, F. Nacimiento, G.G. Ortiz, J.L. Tirado, E. Zhecheva, R. Stoyanova, J. Phys. Chem. C 116 (2012) 20182–20190.
[21] J.R. González, R. Alcántara, G.F. Ortiz, F. Nacimiento, J.L. Tirado, J. Electrochem. Soc. 160 (2013) A1390–A1398.
[22] G.F. Ortiz, I. Hanzu, P. Lavela, P. Knauth, J.L. Tirado, T. Djenizian, Chem. Mater. 22 (2010) 1926–1932.
[23] G.F. Ortiz, I. Hanzu, P. Lavela, J.L. Tirado, P. Knauth, T. Djenizian, J. Mater. Chem. 20 (2010) 4041–4046.
[24] M. Mancini, P. Kubiak, J. Geserick, R. Marassi, N. Hüsing, M. Wohlfahrt-Mehrens, J. Power Sources 189 (2009) 585–589.
[25] W. Chartarrayawadee, S.E. Moulton, D. Li, C.O. Too, G.G. Wallace, Electrochim. Acta 60 (2012) 213–223.
[26] Z. Bi, M.P. Paranthaman, P.A. Menchhofer, R.R. Dehoff, C.A. Bridges, M. Chi, B. Guo, X.G. Suna, S. Dai, J. Power Sources 222 (2013) 461–466.
[27] J.H. Yun, R.J. Wong, Y.H. Ng, A. Du, R. Amal, RSC Adv. 2 (2012) 8164–8171.
[28] C. Botas, P. Álvarez, C. Blanco, M.D. Gutiérrez, P. Ares, R. Zamani, J. Arbiol, J.R. Morante, R. Menéndez, RSC Adv. 2 (2012) 9643–9650.
[29] J. Luo, L.J. Cote, V.C. Tung, A.T.L. Tan, P.E. Goins, J. Wu, J. Huang, J. Am. Chem. Soc. 132 (2010) 17667–17669.
[30] X. Dong, Y. Ma, G. Zhu, Y. Huang, J. Wang, M.B. Chan-Park, L. Wang, W. Huang, P. Chen, J. Mater. Chem. 22 (2012) 1704–17048.
[31] A. Ramadoss, S.J. Kim, Carbon 63 (2013) 434–445.
[32] Y.P. Zhang, J.J. Xu, Z.H. Sun, C.Z. Li, C.X. Pan, Prog. Nat. Sci. 21 (2011) 467–471.
[33] A. Abouimrane, O.C. Compton, K. Amine, S.T. Nguyen, J. Phys. Chem. C 114 (2010) 12800–12804.
[34] L. Liu, H. Liu, Y. Zhang, R. Li, G. Liang, M. Gauthier, X. Sun, Carbon 49 (2011) 5014–5021.
[35] S. Cui, R. Canet, A. Derre, M. Couzi, P. Delhaes, Carbon 41 (2003) 797–809.
[36] H. Xiong, H. Yildrin, E.V. Shevchenko, V.B. Prakapenska, B. Koo, M.D. Slater, M. Balasubramanian, S.K.R.S. Sankaranarayanan, J.P. Greeley, S. Tepavcevic, N.M. Dimitrijevic, P. Podsiadlo, C.S. Johnson, T. Rajh, J. Phys. Chem. C 116 (2012) 3181–3187.
[37] J. Wang, J. Polleux, J. Lim, B. Dunn, J. Phys. Chem. C 111 (2007) 14925–14931.
[38] W.J.H. Borghols, D. Lützenkirchen-Hecht, U. Haake, W. Chan, U. Lafont, E.M. Kelder, E.R.H. van Eck, A.P.M. Kentgens, F.M. Mulder, M.J. Wagemaker, J. Electrochem. Soc. 157 (2010) A582–A588.
[39] M. Marinaro, M. Pfanzelt, P. Kubiak, R. Marassi, M. Wohlfahrt-Mehrens, J. Power Sources 196 (2011) 9825–9829.
[40] Y.K. Zhou, L. Cao, F.B. Zhang, B.L. He, H.L. Li, J. Electrochem. Soc. 150 (2003) A1246–A1249.
[41] F. Nacimiento, J.R. González, R. Alcántara, G.F. Ortiz, J.L. Tirado, J. Electrochem. Soc. 160 (2013) A3026–A3035.